OCEANOGRAPHY

Maintenance of mid-latitude oceanic fronts by mesoscale eddies

Zhao Jing[1,2,3]*, Shengpeng Wang[1,2]*, Lixin Wu[1,2†], Ping Chang[3,4,5], Qiuying Zhang[1,3,4], Bingrong Sun[1,2], Xiaohui Ma[1,2,3], Bo Qiu[6], Justing Small[3,7], Fei-Fei Jin[8], Zhaohui Chen[1,2], Bolan Gan[1,2], Yun Yang[9], Haiyuan Yang[1,2], Xiuquan Wan[1,2]

Oceanic fronts associated with strong western boundary current extensions vent a vast amount of heat into the atmosphere, anchoring mid-latitude storm tracks and facilitating ocean carbon sequestration. However, it remains unclear how the surface heat reservoir is replenished by ocean processes to sustain the atmospheric heat uptake. Using high-resolution climate simulations, we find that the vertical heat transport by ocean mesoscale eddies acts as an important heat supplier to the surface ocean in frontal regions. This vertical eddy heat transport is not accounted for by the prevailing inviscid and adiabatic ocean dynamical theories such as baroclinic instability and frontogenesis but is tightly related to the atmospheric forcing. Strong surface cooling associated with intense winds in winter promotes turbulent mixing in the mixed layer, destructing the vertical shear of mesoscale eddies. The restoring of vertical shear induces an ageostrophic secondary circulation transporting heat from the subsurface to surface ocean.

INTRODUCTION

The intrusion of warm subtropical western boundary current (WBC) extensions, e.g., the Kuroshio extension in the North Pacific, Gulf Stream extension in the North Atlantic, and Agulhas Return Current in the Southern Ocean, into the cold subpolar ocean forms sharp sea surface temperature (SST) fronts. The pronounced horizontal SST gradient in these oceanic frontal regions is crucial for maintaining lower atmospheric baroclinicity and exerts a fundamental influence on mid-latitude climate by enhancing extratropical storm genesis and anchoring the major storm track (*1*–*5*). Moreover, the SST fronts are also the key regions for atmospheric heat and moisture uptake from the ocean (Fig. 1A), as the encountering of the warm sea surface water carried by WBC extensions and the freezing dry air blown from continents by winter storms leads to pronounced sensible and latent heat fluxes (*6*). This strong diabatic heating gives rise to intensified deep convection above the warm flank of the fronts with a locally stronger storm track at low levels along with more explosive cyclogenesis (*4*, *7*, *8*).

The large surface heat loss over WBC extensions in turn acts to erode the SST fronts (*9*, *10*). The subsurface ocean heat reservoir built up by WBCs thus needs to be tapped to maintain the SST fronts (*11*–*13*) against the erosion by atmospheric cooling. Traditionally, the upward heat transport from the subsurface to surface ocean is thought to be mainly achieved by the turbulent vertical mixing triggered by convective instability and wind stirring, as evidenced by the wide usage of mixed layer models to analyze the thermal structures in WBC extensions (*11*–*16*).

Satellite altimeter measurements in the past two decades have revealed energetic mesoscale eddies (*17*) along WBC extensions as a result of strong baroclinic instability of mean flows (*18*). Although it is suggested that these eddies can generate an upward heat transport (*19*–*22*), their contribution to sustaining the sharp SST fronts in WBC extensions remains poorly understood. In particular, it is not uncommon that effects of mesoscale eddies are neglected in recent literature on this issue (*15*, *16*). Moreover, mesoscale eddies are generally beyond the resolution capacity of current-generation climate models (*23*, *24*), so that their induced heat transport needs to be parameterized. However, it is still unknown whether the prevailing parameterizations (*25*, *26*), overlooking the interactions between mesoscale eddies and atmosphere, are applicable to WBC extensions where their interactions are strong and complex. To explore these questions, we analyze the vertical heat transport by mesoscale eddies, its underlying dynamics, and importance in the mixed-layer heat budget in WBC extensions based on high-resolution (0.1°) global climate simulations.

RESULTS

Figure 2 (A to C) shows the winter mean heat flux at the sea surface (defined positive downward in this study) in the Northwest Pacific, Atlantic, and Southern Ocean simulated by the eddy-resolving Community Earth System Model (CESM) simulations developed and conducted by the National Center for Atmospheric Research (see Materials and Methods for model details). Strong ocean heat release occurs in the Kuroshio extension, Gulf Stream extension, and Agulhas Return Current. In contrast, the actual cooling rate of SST averaged over the same period is roughly uniform in the space with no noticeable enhancement along the WBC extensions (Fig. 2, D to F), so that the SST fronts can persist. We remark that such a feature is consistent with that derived from the observed SST and reanalysis heat flux products (fig. S1), providing a validation of the CESM simulations.

[1]Key Laboratory of Physical Oceanography and Frontiers Science Center for Deep Ocean Multispheres and Earth System, Ocean University of China, Qingdao, China. [2]Qingdao National Laboratory for Marine Science and Technology, Qingdao, China. [3]International Laboratory for High-Resolution Earth System Prediction, Texas A&M University, College Station, TX, USA. [4]Department of Oceanography, Texas A&M University, College Station, TX, USA. [5]Department of Atmospheric Sciences, Texas A&M University, College Station, TX, USA. [6]Department of Oceanography, University of Hawaii at Manoa, Honolulu, HI, USA. [7]Climate and Global Dynamics Division, National Center for Atmospheric Research, Boulder, CO, USA. [8]Department of Atmospheric Sciences, University of Hawaii at Manoa, Honolulu, HI, USA. [9]College of Global Change and Earth System Science, Beijing Normal University, Beijing, China.
*These authors contributed equally to this work.
†Corresponding author. Email: lxwu@ouc.edu.cn

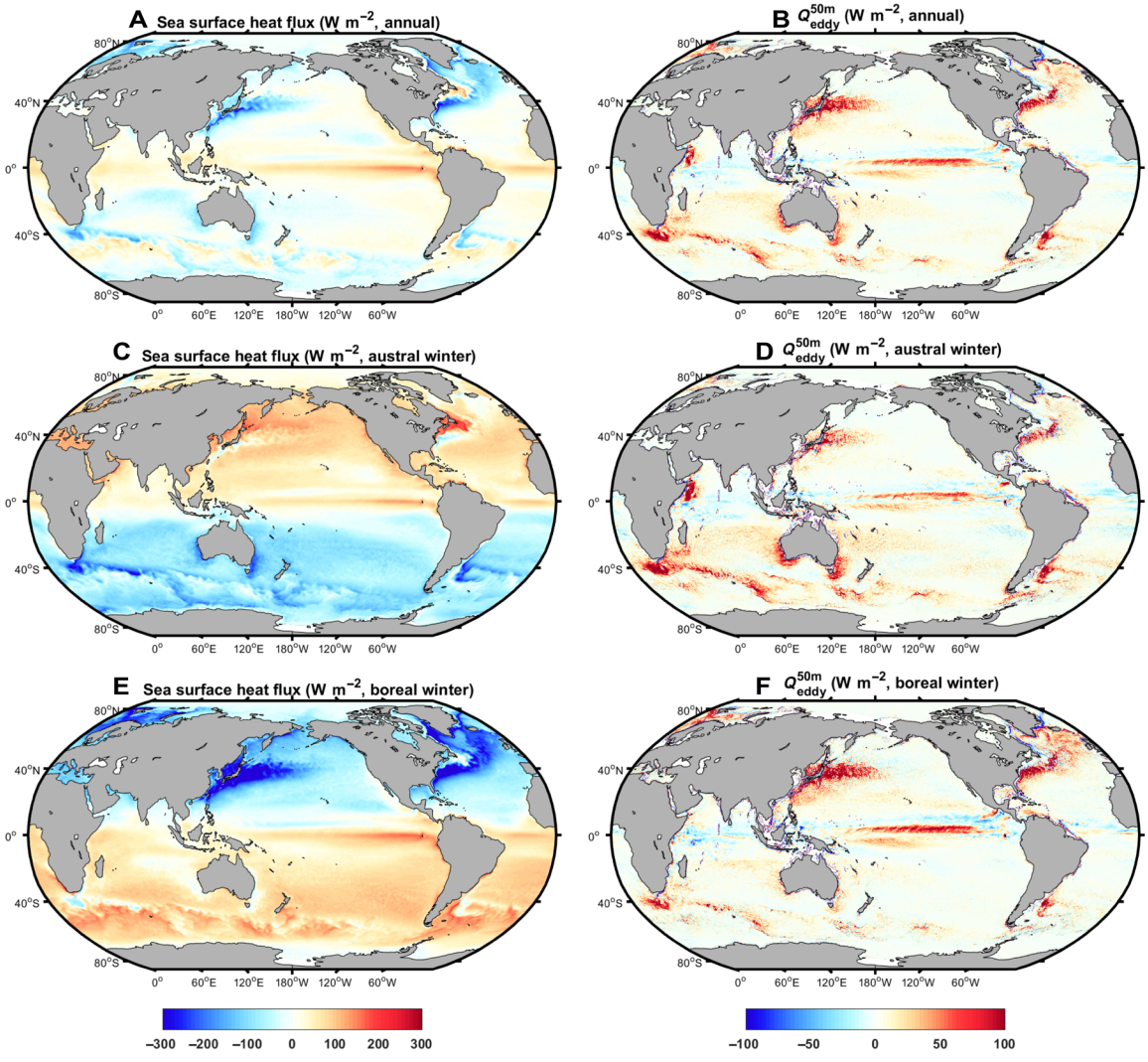

Fig. 1. Coincidence of enhanced atmospheric heat uptake and vertical mesoscale eddy heat transport in WBC extensions. (**A**) Annual mean, (**C**) austral winter mean, and (**E**) boreal winter mean sea surface heat flux (positive downward). **(B**, **D**, and **F**) same as (A), (C), and (E) but for the vertical mesoscale eddy heat transport at 50 m (Q_{eddy}^{50m}). In this study, boreal and austral winters correspond to 1 October to 31 March and 1 April to 30 September, respectively.

The resistance of SST to atmospheric cooling in the WBC extensions implies a strong heat supply by oceanic processes in these regions. To reveal the underlying dynamics responsible for this heat supply, we perform a complete wintertime heat content budget in the WBC extensions using the diagnostic model output from the CESM (Fig. 2, G to I). Here, the budget analysis is restricted to the regions with the winter mean surface heat loss exceeding 300 W m^{-2} in the Kuroshio and Gulf Stream extensions and 150 W m^{-2} in the Agulhas Return Current to highlight the oceanic processes compensating the strong ocean heat release (Fig. 2, A to C). Sensitivity tests show that a slight change of the critical heat flux value does not have a substantial impact on the results. The budget analyses are performed over the upper 50-m layer within which the ocean is almost always well mixed in winter so that the change of layer heat content reflects that of SST.

In the Kuroshio extension, the surface heat flux is −353 W m^{-2} (Fig. 2G), whereas the actual heat content tendency integrated in the upper 50 m is −112 W m^{-2}, comparable to the value in the surrounding region. The difference between the actual heat content tendency and surface heat flux is 241 W m^{-2}, whereas the heat transport convergence of WBCs is only 41 W m^{-2}. Correspondingly, the strong upward heat transport at 50 m is essential to close the heat budget, with the horizontal mesoscale eddy transport convergence and horizontal mixing found to have a minor or negligible influence. The vertical heat transport (Q_{eddy}) by mesoscale eddies plays a fundamental role, contributing as almost equally as that (Q_{turb}) by turbulent vertical mixing. The values of Q_{eddy} and Q_{turb} at 50 m (denoted as Q_{eddy}^{50m} and Q_{turb}^{50m}) are 109 and 95 W m^{-2}, respectively. As the depth increases, Q_{eddy} becomes more dominant because of the rapid attenuation of Q_{turb} (Fig. 3A). For instance, the value of Q_{eddy} doubles that of Q_{turb} at 85 m.

The above findings also hold in the Gulf Stream extension and Agulhas Return Current (Figs. 2, H and I, and 3, B and C). The

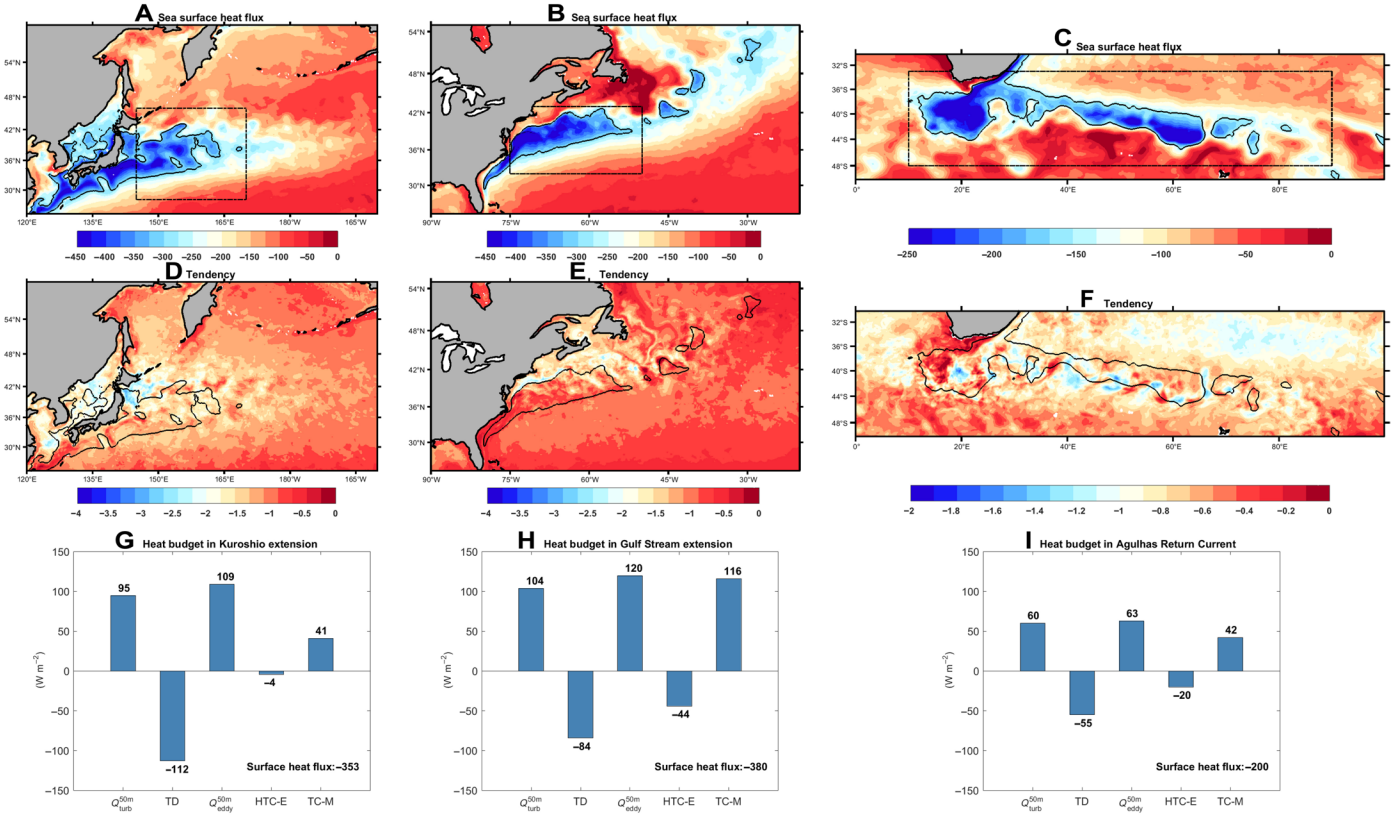

Fig. 2. Ocean heat supply in WBC extensions in winter. Winter mean (**A** to **C**) sea surface heat flux (watt per square meter) and (**D** to **F**) SST tendency (°C per month). (**G** to **I**) Heat content budget in the upper 50 m with TD representing the heat content tendency, TC-M representing the heat transport convergence by the mean flows, HTC-E representing the horizontal mesoscale eddy heat transport convergence, and Q_{eddy} and Q_{turb} representing the vertical heat transport at the lower bound by mesoscale eddies and turbulent vertical mixing. The number in the right lower corner is the area mean surface heat flux that is equal to the minus sum of individual components. The boxes in (A) to (C) enclose the Kuroshio extension, Gulf Stream extension, and Agulhas Return Current. The thick black lines in (A) to (F) denote the contour of critical value (300 W m^{-2} for Kuroshio and Gulf Stream extensions and 150 W m^{-2} for Agulhas Return Current) of winter mean surface heat loss.

values of Q^{50m}_{eddy} and Q^{50m}_{turb} in the Gulf Stream extension (Agulhas Return Current) are 120 and 104 W m^{-2} (63 and 60 W m^{-2}), accounting for 31.6 and 27.4% (31.5 and 30.0%) of the surface heat loss, respectively. Further downward, Q_{eddy} dominates Q_{turb}. On the basis of these heat budget analyses, we conclude that the upward heat transport by mesoscale eddies makes crucial contribution to maintaining the SST fronts against the destruction by the pronounced atmospheric cooling in the WBC extensions.

In the WBC extensions, the winter mean Q_{eddy} exhibits a shallow peak centered around 50 to 70 m (Fig. 3, A to C), making it very efficient to transport heat from the subsurface to surface ocean. This peak cannot be explained by inviscid and adiabatic ocean dynamics such as frontogenesis and baroclinic instability that are found to produce a peak at greater depth with much smaller values (fig. S2). Note that Q^{50m}_{eddy} exhibits a pronounced seasonal cycle with the larger and smaller values occurring in winter and summer, in phase with the seasonal variation of surface heat flux (Figs. 1 and 3). Moreover, the intensity of Q^{50m}_{eddy} within the winter season is strongly modulated by the surface heat flux, as evidenced by their significant coherence at the intraseasonal time scales (Fig. 3). We remark that the tight relationship between Q^{50m}_{eddy} and surface heat flux is unlikely a numerical artifact of CESM as it is consistently reproduced in coupled regional climate simulations (fig. S3).

The strong correlation between Q^{50m}_{eddy} and surface heat flux at the seasonal and intraseasonal time scales (Fig. 3, D to F) implies the importance of viscous or diabatic effect in the underlying dynamics of Q_{eddy}. We hypothesize that strong atmospheric cooling associated with intense winds (there is a tight association between surface heat loss and wind strength; table S1) results in vigorous turbulent mixing in the mixed layer, so that flows of mesoscale eddies are subject to the turbulent thermal wind (TTW) balance (*27*) instead of the classical thermal wind balance (*28*). As the turbulent mixing acts to destroy the vertical shear of mesoscale eddies, an ageostrophic secondary circulation restoring the vertical shear is induced to maintain the TTW balance. It can be proved that the ageostrophic secondary circulation converts eddy available potential energy to eddy kinetic energy, resulting in an upward eddy heat transport peaking in the mixed layer (see the proof in Materials and Methods).

To test this hypothesis, we compare Q_{eddy} and that inferred from the TTW balance, $Q_{eddy\text{-}TTW}$ (Fig. 4). The vertical profiles of winter mean Q_{eddy} and $Q_{eddy\text{-}TTW}$ agree reasonably well in the mixed layer with their peak values differing by less than 15.3/13.8/13.6% in the

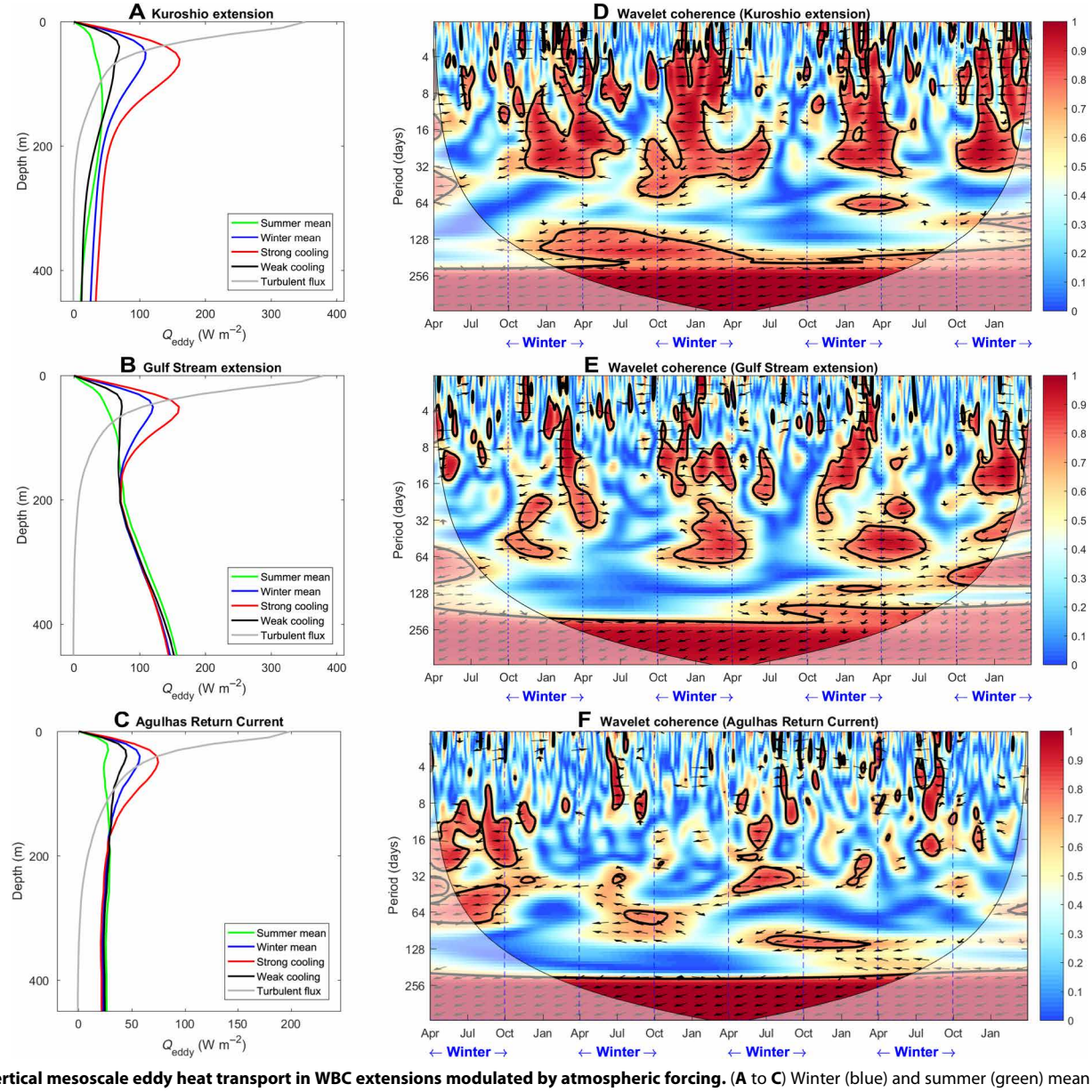

Fig. 3. Vertical mesoscale eddy heat transport in WBC extensions modulated by atmospheric forcing. (**A** to **C**) Winter (blue) and summer (green) mean Q_{eddy}. The black and red lines represent the composite under the weak and strong cooling events in winter. The gray line denotes the winter mean Q_{turb}. Here, the weak (strong) cooling events are defined as the instants with the area mean sea surface heat loss smaller (larger) than the lower (upper) quantile. (**D** to **F**) The wavelet coherence between the time series of sea surface heat flux and Q_{eddy}^{50m}. The coherence significant at the 95% significance level is enclosed by the black solid lines. The arrow indicates the phase lag with pointing rightward (leftward) corresponds to the simultaneous positive (negative) correlation.

Kuroshio extension/Gulf Stream extension/Agulhas Return Current. The temporal variations of Q_{eddy}^{50m} and $Q_{eddy\text{-}TTW}^{50m}$ are also highly consistent with each other in the winter season. Their correlation coefficient reaches up to 0.94/0.92/0.92 in the Kuroshio extension/Gulf Stream extension/Agulhas Return Current ($P < 0.001$). This provides strong evidence that the pronounced peak of Q_{eddy} in the winter mixed layer is due to the ageostrophic secondary circulation associated with the TTW balance. As the intensity of vertical mixing is strongly affected by the atmospheric forcing, this explains the temporal variation of Q_{eddy}^{50m} and its tight relationship to the surface heat flux.

DISCUSSION

This study offers a new perspective on the dynamics sustaining the SST fronts in the WBC extensions (Fig. 5). The oceanic mesoscale eddies and atmospheric synoptic storms form a dynamically coupled system. Intense storms promote the vertical mixing in the mixed layers, leading to enhanced vertical eddy heat transport through the TTW balance. This, in turn, contributes to sustaining the sharp SST fronts, fueling the storm genesis. Such a process cannot be captured by the prevailing mesoscale eddy transport parameterizations (*25*, *26*) in the current generation of climate models. It is important to fully understand how the SST and surface heat flux in WBC extensions would respond to the missing of this vertical mesoscale eddy heat

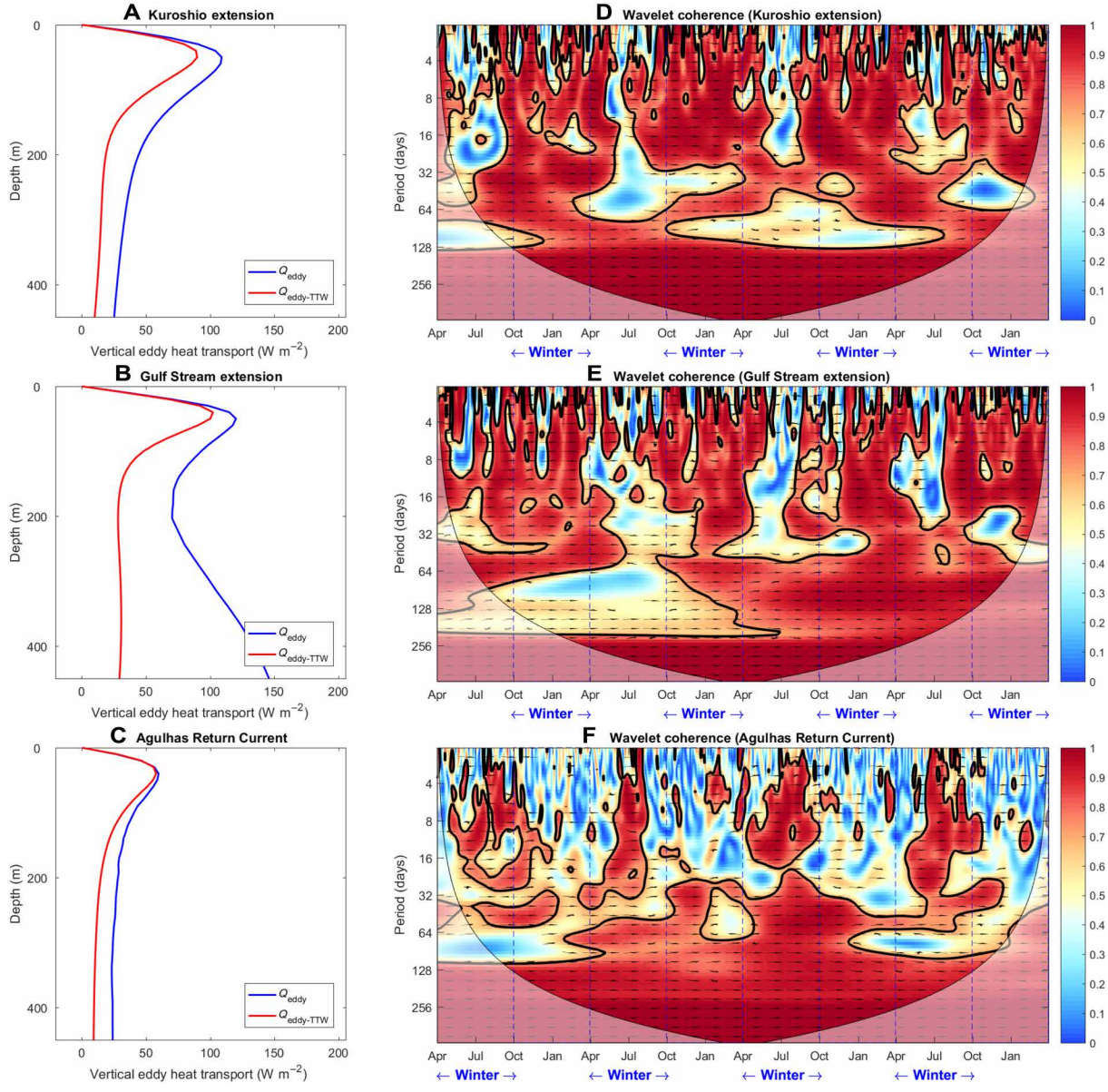

Fig. 4. Contribution of Q_{eddy} from the TTW balance. (**A** to **C**) Winter mean Q_{eddy} (blue) and $Q^{50m}_{eddy\text{-}TTW}$ (red). (**D** to **F**) Wavelet coherence between the time series of $Q^{50m}_{eddy\text{-}TTW}$ and Q^{50m}_{eddy}. The coherence significant at the 95% significance level is enclosed by the black solid lines. The arrows indicate the phase lag with pointing rightward (leftward) corresponding to the simultaneous positive (negative) correlation.

transport triggered by atmospheric forcing. One possibility is that the surface WBC extensions become colder, leading to reduced heat release into the atmosphere. This possibility seems to be supported by comparisons between the high-resolution CESM simulations and that derived from the similar model setting with 1°-resolution ocean component (figs. S4 and S5) (*29*). These responses might have complicated implications on the enhanced surface warming over the past century in WBC extensions (*30*), as well as the carbon dioxide uptake and fishery yields there through the marked influences of SST on the solubility of carbon dioxide of seawater (*31*) and the activities of organisms in the euphotic zone (*32*). Furthermore, it is found that the important role of the TTW balance in generating the upper-ocean vertical mesoscale eddy heat transport is not only confined to WBC extensions but throughout the off-equatorial regions (fig. S6). This may partially account for the pronounced peak of vertical eddy heat transport in the upper ocean reported in previous mesoscale eddy–resolving simulations (*22*, *33*, *34*). Last, we remark that the climate models used in this study do not resolve eddies at submesoscales. Although resolving these submesoscale eddies remains probably unaccomplishable for the long-term global climate simulations in the coming decade, they are suggested to contribute notably to the vertical heat transport in the mixed layer through baroclinic instability, frontogenesis (*35*, *36*), and possibly the mechanism documented in this study. Therefore, our study is likely to provide a conservative estimate of role of oceanic eddies in maintaining the fronts.

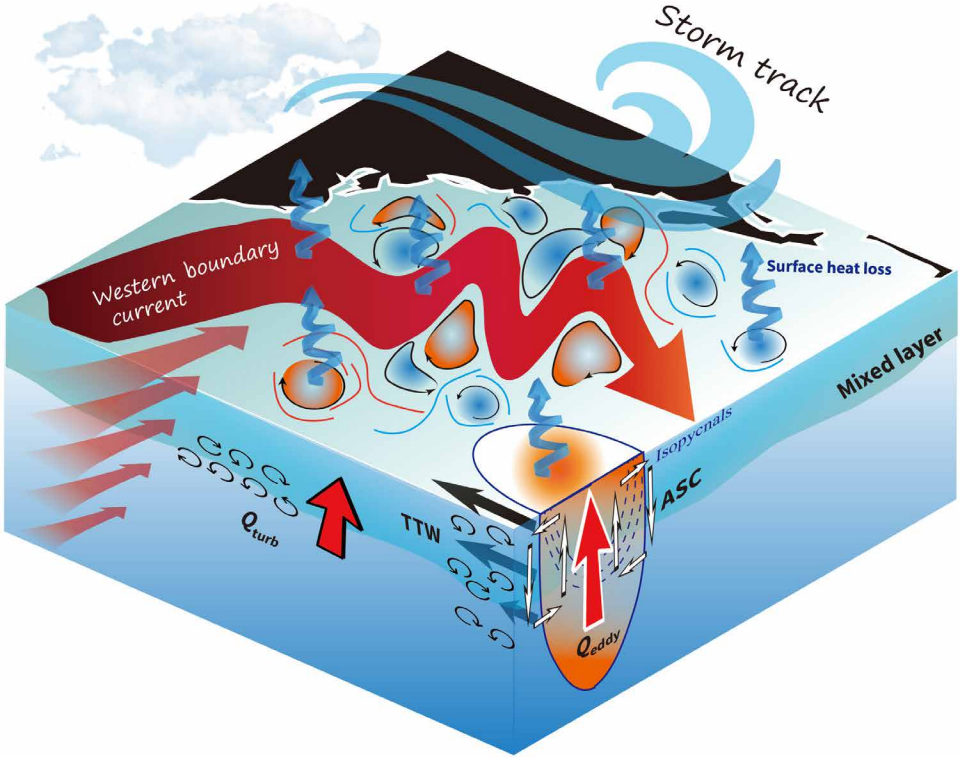

Fig. 5. Schematic of dynamics for the enhanced vertical mesoscale eddy heat transport by winter storms. WBC extensions have abundant mesoscale eddies including coherent vortices, as well as a rich cascade of other structures such as filaments, squirts, and spirals. These mesoscale eddies and atmospheric synoptic storms form a dynamically coupled system. Passage of winter storms leads to strong atmospheric cooling associated with intensified winds. It enhances turbulent mixing in the mixed layer and destroys the vertical shear of mesoscale eddies, leading to an ageostrophic secondary circulation (ASC) restoring the TTW balance and transporting heat upward (see the white arrows in a zoomed-in circular coherent vortex as an illustration example). This, in turn, contributes to sustaining the sharp SST fronts, fueling the storm genesis.

MATERIALS AND METHODS

Model configuration

The global simulations are conducted using the CESM. It includes the Community Atmosphere Model version 5 (CAM5) as its atmospheric component and Parallel Ocean Program version 2 (POP2) as its oceanic component. The horizontal resolutions of CAM5 and POP2 are around 0.25° and 0.1°, respectively. For POP2, there are 62 levels in the vertical direction with increasing grid space from 5 m near the sea surface to 250 m near the bottom. The Laplacian viscosity (diffusion) coefficient is set as $1 \times 10^4\ m^2\ s^{-1}$ ($1 \times 10^4\ m^2\ s^{-1}$), and the biharmonic viscosity (diffusion) coefficient is set as $27 \times 10^9\ m^4\ s^{-1}$ ($3 \times 10^9\ m^4\ s^{-1}$). The ocean model provides SST and surface current to the atmosphere model and receives updated fluxes from the atmosphere model calculated using the Large and Yeager surface layer scheme every 6 hours (*37*). CESM is integrated for 105 years with 15 years of spin-up. From 1 April 1987 to 31 March 1991, daily averaged temperature, salinity, three-dimensional (3D) velocity, surface fluxes, and diagnostic terms are saved and used in this study.

To assess the validity of the results derived from the CESM simulations, we repeat the analyses based on an ensemble of regional simulations in the North Pacific from the coupled regional climate model (CRCM) developed at Texas A&M University. It includes the Weather Research and Forecasting model as the atmospheric component and Regional Ocean Modeling System as the oceanic component. The two models are coupled every 1 hour, and both have a horizontal resolution of 9 km. The CRCM simulations consist of an ensemble of five 6-month integrations, initialized on 1 October 2003, 2004, 2005, 2006, and 2007, respectively. More details can be found in Ma *et al.* (*38*).

Isolation of mesoscale eddy signals

Mesoscale eddies are defined as perturbations from the seasonal mean of individual years. That is, the winter (summer) mean value of some year is subtracted from original time series in winter (summer) of the same year. Such a definition simplifies the heat budget analysis in winter (see next subsection) due to the vanishing covariance terms of mesoscale eddies and mean flows and facilitates the comparison of vertical eddy heat transport between winter and summer.

Mesoscale eddies defined in the above way are contaminated by large-scale variability at intraseasonal time scales. We find the contamination negligible, as evidenced by the decomposition of Q_{eddy}^{50m} in the horizontal wave number space in WBC extensions (fig. S7). In these regions, motions with horizontal wavelength shorter than 300 km account for about 95% of Q_{eddy}^{50m}.

Heat content budget in the upper ocean

The heat content budget in the upper ocean can be derived as

$$\left\langle \int_{-h}^{0} \rho_0 C_P \frac{\partial T}{\partial t} dz \right\rangle = -\left\langle \int_{-h}^{0} \rho_0 C_P \nabla \cdot (\overline{\mathbf{u}}\,\overline{T})\, dz \right\rangle - \left\langle \int_{-h}^{0} \rho_0 C_P \nabla_h \cdot (\mathbf{u}_h' T')\, dz \right\rangle + \left\langle \int_{-h}^{0} \rho_0 C_P \kappa_h \nabla_h^2 T dz - \int_{-h}^{0} \rho_0 C_P \kappa_4 \nabla_h^4 T dz \right\rangle + \langle Q_{surf} \rangle + \left\langle Q_{eddy}|_{z=-h} \right\rangle + \left\langle Q_{turb}|_{z=-h} \right\rangle \quad (1)$$

where T is the temperature, $\mathbf{u} = (\mathbf{u}_h, w)$ is the 3D velocity vector with $\mathbf{u}_h = (u, v)$ its horizontal component and w the vertical component, $\nabla = (\partial/\partial x, \partial/\partial y, \partial/\partial z)$, $\nabla_h = (\partial/\partial x, \partial/\partial y)$, κ_h is the horizontal diffusion coefficient, κ_4 is the horizontal biharmonic diffusion coefficient, $\rho_0 = 1027.5$ kg m^{-3} is the ocean reference density, C_p is the ocean specific heat capacity, Q_{surf} is the sea surface heat flux defined positive downward, $Q_{eddy} = \rho_0 C_P w'T'$ and Q_{turb} are the vertical heat transport (defined positive upward) by mesoscale eddies and turbulent vertical mixing, respectively, h is the lower bound for the vertical integration, and $\langle \ldots \rangle$ denotes a time average in the winter season of multiple years plus a spatial average over the region with the surface heat loss exceeding 300 W m^{-2} in the Kuroshio and Gulf Stream extensions and 150 W m^{-2} in the Agulhas Return Current (Fig. 2). The prime and overbar represent the mesoscale eddies and mean flows, respectively.

The term on the left-hand side of Eq. 1 is the heat content tendency (denoted as TD), which is balanced by terms on the right-hand side of Eq. 1. The first term on the right-hand side is the heat transport convergence by the mean flows (denoted as TC-M). The second represents the horizontal mesoscale eddy heat transport convergence (denoted as HTC-E). The third is the horizontal turbulent mixing. The fourth represents the sea surface heat flux. The fifth and sixth are the vertical heat transport at the lower bound by mesoscale eddies and turbulent vertical mixing. These terms are computed using the daily averaged diagnostic output from the CESM simulations. Note that the horizontal turbulent mixing term is more than an order of magnitude smaller than the other terms in Eq. 1 and will be dropped in the following analysis.

TTW and associated vertical eddy heat transport

The TTW balance (*27*) is the balance between the Coriolis force, horizontal pressure gradient, and vertical mixing of momentum, i.e.

$$0 = fv - \frac{1}{\rho_0}\frac{\partial p}{\partial x} + \frac{\partial}{\partial z}\left(K_m \frac{\partial u}{\partial z}\right) \quad (2)$$

$$0 = -fu - \frac{1}{\rho_0}\frac{\partial p}{\partial y} + \frac{\partial}{\partial z}\left(K_m \frac{\partial v}{\partial z}\right) \quad (3)$$

where K_m is the vertical viscosity, f is the Coriolis parameter, and p is the hydrostatic pressure. Adopting the rigid lid approximation for the sea surface, the vertical velocity can be derived as

$$w_{TTW} = \frac{1}{f\rho_0}\left(\frac{\partial}{\partial x}\tau_y - \frac{\partial}{\partial y}\tau_x\right) - \frac{1}{f}\left(\frac{\partial}{\partial x}K_m\frac{\partial v}{\partial z} - \frac{\partial}{\partial y}K_m\frac{\partial u}{\partial z}\right) \quad (4)$$

where $\boldsymbol{\tau} = (\tau_x, \tau_y)$ is the surface wind stress. The associated vertical eddy heat transport, $Q_{eddy\text{-}TTW}$, can be computed as

$$Q_{eddy\text{-}TTW} = \rho_0 C_P w_{TTW}'T' \quad (5)$$

As it is the density (ρ) or buoyancy ($b = -\frac{g}{\rho_0}\rho$) instead of temperature that directly affects the motions of fluids, we will use the vertical eddy buoyancy transport ($B_{eddy\text{-}TTW} = w_{TTW}'\,b'$) as a proxy for $Q_{eddy\text{-}TTW}$ to facilitate the dynamical analysis. The buoyancy change is dominated by the temperature change in WBC extensions. After some manipulations, the regional mean vertical eddy buoyancy transport, $\langle B_{eddy\text{-}TTW}\rangle_S$, can be expressed as

$$\langle B_{eddy\text{-}TTW}\rangle_S = \langle w_{TTW}'b'\rangle_S = \frac{1}{A}\oint \frac{b'}{f}\left(\frac{\boldsymbol{\tau}}{\rho_0} - K_m\frac{\partial \mathbf{u}_h}{\partial z}\right)' d\boldsymbol{l} - \left\langle \frac{\boldsymbol{\tau}'}{\rho_0}\frac{\partial \mathbf{u}_g'}{\partial z}\right\rangle_S + \left\langle \left(K_m\frac{\partial \mathbf{u}_h}{\partial z}\right)', \frac{\partial \mathbf{u}_g'}{\partial z}\right\rangle_S \quad (6)$$

where A is the area of the region, $d\boldsymbol{l}$ is the line element along the boundaries, $\mathbf{u}_g = (u_g, v_g)$ is the geostrophic flow, and $\frac{\partial \mathbf{u}_g}{\partial z}$ is the geostrophic shear. To derive Eq. 6, f is treated as a slowly varying parameter with terms proportional to its meridional derivative neglected.

The first term on the right-hand side of Eq. 6 represents the boundary effect ($B_{eddy\text{-}TTW\text{-}boundary}$) that is found to be negligible. The second term, related to the wind power on geostrophic flows ($B_{eddy\text{-}TTW\text{-}wind}$), makes minor contribution. The third term, the destruction of shear by vertical mixing ($B_{eddy\text{-}TTW\text{-}mixing}$), dominates $B_{eddy\text{-}TTW}$ (fig. S8).

Assessing the contribution of Q_{eddy} from inviscid and adiabatic ocean dynamics

An omega equation based on semigeostrophic dynamics (*39*, *40*) is used to isolate the contribution of Q_{eddy} from inviscid and adiabatic ocean dynamics (including but not limited to frontogenesis and baroclinic instability)

$$f^2\frac{\partial^2 w_{SQG}}{\partial z^2} + \nabla_h \cdot \left(\frac{\partial b}{\partial z}\nabla_h w_{SQG}\right) = 2\nabla_h \cdot \mathbf{Q} + \nabla_h \cdot \mathbf{A} \quad (7)$$

$$\mathbf{Q} = -\left(\frac{\partial u_g}{\partial x}\frac{\partial b}{\partial x} + \frac{\partial v_g}{\partial x}\frac{\partial b}{\partial y}, \frac{\partial u_g}{\partial y}\frac{\partial b}{\partial x} + \frac{\partial v_g}{\partial y}\frac{\partial b}{\partial y}\right)$$

$$\mathbf{A} = \left(f\frac{\partial \mathbf{u}_{ah}}{\partial z}\cdot\nabla_h v_g - 2\frac{\partial u_a}{\partial x}\frac{\partial b}{\partial x} - \frac{\partial v_a}{\partial x}\frac{\partial b}{\partial y} - \frac{\partial v_a}{\partial y}\frac{\partial b}{\partial x}, -f\frac{\partial \mathbf{u}_{ah}}{\partial z}\cdot\nabla_h u_g - \frac{\partial u_a}{\partial y}\frac{\partial b}{\partial x} - 2\frac{\partial v_a}{\partial y}\frac{\partial b}{\partial y} - \frac{\partial u_a}{\partial x}\frac{\partial b}{\partial y}\right)$$

where the solution w_{SQG} represents the contribution of w from inviscid and adiabatic semigeostrophic ocean dynamics and $\mathbf{u}_{ah} = (u_a, v_a) = (u - u_g, v - v_g)$ is the horizontal component of ageostrophic flows. The omega equation is solved in the upper 500 m of WBC regions using successive over relaxation methods with Chebyshev acceleration. The value of $\frac{\partial b}{\partial z}$ is limited larger than the threshold $\frac{\partial b}{\partial z}|_{min} = 1 \times 10^{-9}$ s^{-2} to ensure the astringency of the algorithm. The results are found insensitive to the value of threshold provided that it is positive and reasonably small. The contribution of Q_{eddy} from w_{SQG}, $Q_{eddy\text{-}SQG}$, can be computed as

$$Q_{eddy\text{-}SQG} = \rho_0 C_P w_{SQG}'T' \quad (8)$$

SUPPLEMENTARY MATERIALS

Supplementary material for this article is available at http://advances.sciencemag.org/cgi/content/full/6/31/eaba7880/DC1

REFERENCES AND NOTES

1. T. M. Joyce, Y.-O. Kwon, L. Yu, On the relationship between synoptic wintertime atmospheric variability and path shifts in the Gulf Stream and the Kuroshio Extension. *J. Climate* **22**, 3177–3192 (2009).
2. C. H. O'Reilly, A. Czaja, The response of the pacific storm track and atmospheric circulation to Kuroshio Extension variability. *Q. J. Roy. Meteorol. Soc.* **141**, 52–66 (2015).
3. D. Hotta, H. Nakamura, On the significance of the sensible heat supply from the ocean in the maintenance of the mean baroclinicity along storm tracks. *J. Climate* **24**, 3377–3401 (2011).
4. R. J. Small, R. A. Tomas, F. O. Bryan, Storm track response to ocean fronts in a global high-resolution climate model. *Clim. Dynam.* **43**, 805–828 (2014).
5. D. Hu, L. Wu, W. Cai, A. S. Gupta, A. Ganachaud, B. Qiu, A. L. Gordon, X. Lin, Z. Chen, S. Hu, Pacific western boundary currents and their roles in climate. *Nature* **522**, 299–308 (2015).
6. G. W. K. Moore, I. A. Renfrew, An assessment of the surface turbulent heat fluxes from the NCEP–NCAR reanalysis over the western boundary currents. *J. Climate* **15**, 2020–2037 (2002).
7. H. Tokinaga, Y. Tanimoto, S.-P. Xie, T. Sampe, H. Tomita, H. Ichikawa, Ocean frontal effects on the vertical development of clouds over the western North Pacific: In situ and satellite observations. *J. Climate* **22**, 4241–4260 (2009).
8. A. Kuwano-Yoshida, S. Minobe, Storm-track response to SST fronts in the northwestern Pacific region in an AGCM. *J. Climate* **30**, 1081–1102 (2017).
9. S. Dong, S. T. Gille, J. Sprintall, An assessment of the Southern Ocean mixed layer heat budget. *J. Climate* **20**, 4425–4442 (2007).
10. M. Nonaka, H. Nakamura, B. Taguchi, N. Komori, A. Kuwano-Yoshida, K. Takaya, Air–sea heat exchanges characteristic of a prominent midlatitude oceanic front in the South Indian Ocean as simulated in a high-resolution coupled GCM. *J. Climate* **22**, 6515–6535 (2009).
11. F. Vivier, K. A. Kelly, L. A. Thompson, Heat budget in the Kuroshio Extension region: 1993–99. *J. Phys. Oceanogr.* **32**, 3436–3454 (2002).
12. K. A. Kelly, S. Dong, The relationship of western boundary current heat transport and storage to midlatitude ocean-atmosphere interaction. *Earth's Clim.* **147**, 347–363 (2004).
13. S. Dong, K. A. Kelly, Heat budget in the Gulf Stream region: The importance of heat storage and advection. *J. Phys. Oceanogr.* **34**, 1214–1231 (2004).
14. F. Vivier, D. Iudicone, F. Busdraghi, Y.-H. Park, Dynamics of sea-surface temperature anomalies in the Southern Ocean diagnosed from a 2D mixed-layer model. *Clim. Dynam.* **34**, 153–184 (2010).
15. T. Tozuka, M. F. Cronin, Role of mixed layer depth in surface frontogenesis: The Agulhas Return Current front. *Geophys. Res. Lett.* **41**, 2447–2453 (2014).
16. T. Tozuka, M. F. Cronin, H. Tomita, Surface frontogenesis by surface heat fluxes in the upstream Kuroshio Extension region. *Sci. Rep.* **7**, 10258 (2017).
17. The terminology "mesoscale eddies" in this manuscript refers to all kinds of structures at mesoscale (a few tens of kilometers to several hundreds of kilometers) including coherent vortices, as well as a rich cascade of other structures like filaments, squirts, and spirals.
18. A. Gill, J. Green, A. Simmons, Energy partition in the large-scale ocean circulation and the production of mid-ocean eddies. *Deep Sea Res. Oceanogr. Abst.* **21**, 499–528 (1974).
19. I. Orlanski, M. D. Cox, Baroclinic instability in ocean currents. *Geophys. Astrophys. Fluid Dyn.* **4**, 297–332 (1972).
20. A. R. Robinson, J. C. McWilliams, The baroclinic instability of the open ocean. *J. Phys. Oceanogr.* **4**, 281–294 (1974).
21. B. J. Hoskins, The mathematical theory of frontogenesis. *Annu. Rev. Fluid Mech.* **14**, 131–151 (1982).
22. S. M. Griffies, M. Winton, W. G. Anderson, R. Benson, T. L. Delworth, C. O. Dufour, J. P. Dunne, P. Goddard, A. K. Morrison, A. Rosati, Impacts on ocean heat from transient mesoscale eddies in a hierarchy of climate models. *J. Climate* **28**, 952–977 (2015).
23. R. Knutti, J. Sedláček, Robustness and uncertainties in the new CMIP5 climate model projections. *Nat. Clim. Change* **3**, 369 (2013).
24. T. F. Stocker, D. Qin, G.-K. Plattner, M. Tignor, S. K. Allen, J. Boschung, A. Nauels, Y. Xia, V. Bex, P. M. Midgley, *The Physical Science Basis* (Cambridge Univ. Press, 2013).
25. P. R. Gent, J. C. Mcwilliams, Isopycnal mixing in ocean circulation models. *J. Phys. Oceanogr.* **20**, 150–155 (1990).
26. R. Ferrari, J. C. McWilliams, V. M. Canuto, M. Dubovikov, Parameterization of eddy fluxes near oceanic boundaries. *J. Climate* **21**, 2770–2789 (2008).
27. J. Gula, M. J. Molemaker, J. C. McWilliams, Submesoscale cold filaments in the Gulf Stream. *J. Phys. Oceanogr.* **44**, 2617–2643 (2014).
28. J. Pedlosky, *Geophysical Fluid Dynamics* (Springer Science & Business Media, 2013).
29. R. J. Small, R. Msadek, Y.-O. Kwon, J. F. Booth, C. Zarzycki, Atmosphere surface storm track response to resolved ocean mesoscale in two sets of global climate model experiments. *Climate Dynam.* **52**, 2067–2089 (2019).
30. L. Wu, W. Cai, L. Zhang, H. Nakamura, A. Timmermann, T. Joyce, M. J. McPhaden, M. Alexander, B. Qiu, M. Visbeck, Enhanced warming over the global subtropical western boundary currents. *Nat. Clim. Change* **2**, 161–166 (2012).
31. J. L. Sarmiento, N. Gruber, *Ocean Biogeochemical Dynamics* (Princeton Univ. Press, 2006).
32. J. Wohlers, A. Engel, E. Zöllner, P. Breithaupt, K. Jürgens, H.-G. Hoppe, U. Sommer, U. Riebesell, Changes in biogenic carbon flow in response to sea surface warming. *Proc. Natl. Acad. Sci. U.S.A.* **106**, 7067–7072 (2009).
33. C. L. Wolfe, P. Cessi, J. L. McClean, M. E. Maltrud, Vertical heat transport in eddying ocean models. *Geophys. Res. Lett.* **35**, L23605 (2008).
34. A. Morrison, O. Saenko, A. M. Hogg, P. Spence, The role of vertical eddy flux in Southern Ocean heat uptake. *Geophys. Res. Lett.* **40**, 5445–5450 (2013).
35. G. Boccaletti, R. Ferrari, B. Fox-Kemper, Mixed layer instabilities and restratification. *J. Phys. Oceanogr.* **37**, 2228–2250 (2007).
36. J. C. McWilliams, Submesoscale currents in the ocean. *Proc. Math. Phys. Eng. Sci.* **472**, 20160117 (2016).
37. R. J. Small, J. Bacmeister, D. Bailey, A. Baker, S. Bishop, F. Bryan, J. Caron, J. Dennis, P. Gent, H.-m. Hsu, M. Jochum, D. Lawrence, E. Muñoz, P. diNezio, T. Scheitlin, R. Tomas, J. Tribbia, Y.-h. Tseng, M. Vertenstein, A new synoptic scale resolving global climate simulation using the Community Earth System Model. *J. Adv. Model. Earth Syst.* **6**, 1065–1094 (2014).
38. X. Ma, Z. Jing, P. Chang, X. Liu, R. Montuoro, R. J. Small, F. O. Bryan, R. J. Greatbatch, P. Brandt, D. Wu, X. Lin, L. Wu, Western boundary currents regulated by interaction between ocean eddies and the atmosphere. *Nature* **535**, 533–537 (2016).
39. B. J. Hoskins, The geostrophic momentum approximation and the semi-geostrophic equations. *J. Atmos. Sci.* **32**, 233–242 (1975).
40. J.-M. Pinot, J. Tintoré, D.-P. Wang, A study of the omega equation for diagnosing vertical motions at ocean fronts. *J. Mar. Res.* **54**, 239–259 (1996).

Acknowledgments

Funding: This work was supported by the National Natural Science Foundation of China (41490643, 41490640, 41521091, 41776006, and 41822601). Computation for the work described in this paper was supported by the Texas Advanced Computing Center at the University of Texas at Austin, Texas A&M High Performance Research Computing, and the Center for High Performance Computing and System Simulation, Qingdao National Laboratory for Marine Science and Technology. This research is completed through the International Laboratory for High Resolution Earth System Prediction, a collaboration by the Qingdao National Laboratory for Marine Science and Technology Development Center, Texas A&M University, and the National Center for Atmospheric Research. **Author contributions:** Z.J. proposed the central idea and wrote the manuscript. S.W. conducted the analysis under Z.J.'s instruction. L.W. led the research and organized the writing of the manuscript. P.C. contributed to the writing of the manuscript and was involved in interpreting the results. Q.Z. performed the CESM simulations. B.S. and X.M. performed the CRCM simulations. B.Q., J.S., F.-F.J., Z.C., B.G., Y.Y., H.Y., and X.W. contributed to improving the manuscript. **Competing interests:** The authors declare that they have no competing interests. **Data and materials availability:** All data needed to evaluate the conclusions in the paper are present in the paper and/or the Supplementary Materials, as well as references cited therein. Additional data related to this paper may be requested from the authors.

Submitted 6 January 2020
Accepted 19 June 2020
Published 31 July 2020
10.1126/sciadv.aba7880

Citation: Z. Jing, S. Wang, L. Wu, P. Chang, Q. Zhang, B. Sun, X. Ma, B. Qiu, J. Small, F.-F. Jin, Z. Chen, B. Gan, Y. Yang, H. Yang, X. Wan, Maintenance of mid-latitude oceanic fronts by mesoscale eddies. *Sci. Adv.* **6**, eaba7880 (2020).

Science Advances

Maintenance of mid-latitude oceanic fronts by mesoscale eddies

Zhao Jing, Shengpeng Wang, Lixin Wu, Ping Chang, Qiuying Zhang, Bingrong Sun, Xiaohui Ma, Bo Qiu, Justing Small, Fei-Fei Jin, Zhaohui Chen, Bolan Gan, Yun Yang, Haiyuan Yang and Xiuquan Wan

Sci Adv **6** (31), eaba7880.
DOI: 10.1126/sciadv.aba7880

Science Advances (ISSN 2375-2548) is published by the American Association for the Advancement of Science, 1200 New York Avenue NW, Washington, DC 20005. The title *Science Advances* is a registered trademark of AAAS.